JOURNAL OF PROPULSION AND POWER
Vol. 23, No. 1, January–February 2007

Interaction Between Solid Rocket Motor Internal Flow and Structure During Flight

Kirk W. Dotson* and Brian H. Sako†
The Aerospace Corporation, Los Angeles, California, 90009-2957

DOI: 10.2514/1.20477

Measurements of solid rocket motor head end pressure and structural acceleration recorded during flights of a heavy lift launch vehicle are used to investigate if an interaction between the motor internal flow and structural motion exists. These data reveal that a locking of frequency and phase occurs over a 34-s period towards the end of the motor burn. A feedback relationship involving the motor pressure oscillations and structural accelerations, therefore, exists for this launch vehicle. The observed interaction significantly increases the pressure oscillation amplitudes relative to those measured in ground tests at the same burn time. This finding highlights a limitation of motor stability analysis methodology, in which structural motion is traditionally neglected. It appears that the potential for coupling between the motor pressure oscillations and structural response should be accounted for in predictions of solid rocket motor stability. The observed interaction also has implications for the prediction of loads induced by solid rocket motor pressure oscillations. Under some conditions the use of forcing functions based solely on ground test pressure measurements may underpredict flight loads.

Nomenclature

a	=	acceleration signal, g
$\hat{a}$	=	Hilbert transform of a, g
f'	=	generalized force normalized with respect to unit lb_m, $in./s^2$
q	=	modal structural displacement, in.
t	=	time after ignition (burn time), s
x	=	structural displacement; also, oscillatory pressure normalized with respect to gas weight density, in.
ζ_o, ζ_e	=	nominal and effective damping (as a ratio to the critical value), dimensionless
θ	=	phase, rad
ϕ	=	phase difference between structural velocity and fluid force, rad
ω_o, ω_e	=	nominal and effective circular natural frequency, rad/s

I. Introduction

PRESSURE oscillations occur during the burning of propellants in rocket motors. The dynamic environment induced by this phenomenon causes structural oscillations that may exceed in amplitude those from other events that occur during the flight of the launch vehicle. It will be shown that solid rocket motor internal flow may also interact with the structural oscillations, such that a feedback loop is established.

Pressure oscillations internal to solid rocket motors have received much attention in the propulsion community. The oscillations have conventionally been viewed as manifestations of instability induced strictly by combustion or fluid mechanical processes [1]. That is, the theory and codes that exist for the prediction of solid rocket motor stability are based on the energy sources and the energy dissipation within the combustion chamber that occur even in the absence of structural oscillations [2–4]. Unlike liquid rocket engines, stability in solid rocket motors has traditionally been predicted without taking into account potential interactions between the pressure and structural responses.

The methodology presented by Dotson et al. [5] appears to be the only published attempt to address the analytical prediction of structural loads induced by solid rocket motor pressure oscillations. In this approach, data acquired during ground tests (static firings) of the solid rocket motor are used to develop forcing functions, which are applied to the structural model. Responses induced by solid rocket motor pressure oscillations are predicted for a Taurus mission and are compared with those for liftoff and aerodynamic buffeting.

It is assumed in [5] that the motor pressure and structural responses do not interact, and a clear correspondence between ground and flight pressure oscillations is expected. In a technical comment written in response to [5], Hessler and Glick [6] question the generality of these assumptions and call attention to the theory of Deur and Hessler [7], which was developed to predict solid rocket motor stability and pressure oscillation amplitudes, including structural participation. This paper elaborates on the brief response to the technical comment [8], and investigates whether an interaction between motor pressure and structural responses is evident in extant flight data for the Titan IV launch vehicle.

II. Motor Fluid–Structure Interaction

The distinction between forces that are coupled with the acoustic system and forces that are independent of pressure is drawn in this section.

When nonacoustic perturbations are considered, the equations for pressure oscillations in solid rocket motors have the same form as a set of mechanical oscillators undergoing forced excitation [9]. The equation of motion for a single acoustic mode can be written as

$$\ddot{x} + 2\zeta_o\omega_o\dot{x} + \omega_o^2 x = f'(t) + f'(x, \dot{x}, \ddot{x}) \tag{1}$$

The generalized forces on the right-hand side of Eq. (1) specifically include forces caused by combustion noise, turbulence, vortices, axial structural acceleration, and port dilation [7,9]. Other causes may also be possible. Of these generalized forces, only those due to combustion noise are always independent of the normalized pressure amplitude (that is, acoustic displacement) x. The other forces commonly have components that are dependent on x, but under various conditions may also have components that are independent of x [10,11]. Conditions leading to components

Presented as Paper 4183 at the 40th AIAA/ASME/SAE/ASEE Joint Propulsion Conference, Fort Lauderdale, FL, 11–14 July 2004; received 11 October 2005; revision received 7 June 2006; accepted for publication 23 June 2006.

*Senior Engineering Specialist. Structural Dynamics Department, P.O. Box 92957-M4/911. Associate Fellow AIAA.

†Senior Engineering Specialist. Structural Dynamics Department, P.O. Box 92957-M4/911.

independent of x include turbulence caused by vorticity production in the combustion zone, axial acceleration or port dilation due to airloading in flight, deliberate pulsing in ground tests or thrust vector control, and the contributions of these force components or combustion noise forces to vortex formation [7,9].

If the generalized forces that are functions of the normalized pressure oscillations $x(t)$ and its derivatives are moved to the left-hand side, Eq. (1) can be expressed as

$$\ddot{x} + 2\zeta_e\omega_e\dot{x} + \omega_e^2 x = f'(t) \tag{2}$$

where the effective frequency and damping values differ from the nominal values due to the pressure-dependent force terms. Note that a negative value of effective system damping may result if the pressure-dependent force terms are large in amplitude and are in phase with the first derivative of x. In this case, the forces in effect pump energy into the acoustic system. Note also that pressure oscillations will occur due to excitation from the force components that are independent of x, regardless of the damping coefficient.

Equation (2) is heuristic, and it is not suggested that time-domain analyses should be conducted for the subject problem. In a broad range of fluid–structure interaction phenomena, equations of motion like Eq. (2) are formulated and evaluated in the frequency domain.

The effects of the forces due to structural accelerations are of primary interest in this work. That is, if the pressure oscillations are influenced significantly by structural oscillations, then it may be inappropriate to rely on forcing functions developed from ground test data to predict flight responses. This key issue was raised in the technical comment by Hessler and Glick [6].

The term "forced oscillation" is generally applied only if the external forces are independent of the resulting motion. The use of this term in [7] appears to have caused confusion in the combustion instability community, and has led some investigators to conclude that all of the forcing functions developed by Deur and Hessler [7] are uncoupled from oscillatory pressure.

Evidence in flight data of coupling between motor pressure oscillations and structural accelerations will be referred to herein as *fluid–structure interaction*. These oscillations may be self-sustaining but, nevertheless, arise only in the presence of a causative force such as combustion noise [$f'(t)$ in Eq. (2)]. Structural excitation due to pressure oscillations without evidence of coupling will be referred to herein as *forced oscillation*.

III. Titan IV Flight Data

In this section, an investigation of fluid–structure interaction in solid rocket motors is conducted using flight measurements for the Titan IV Solid Motor Upgrade (SRMU). These data are compared with those from static firings of the SRMU. The Titan IV launch vehicle has flown 37 times since its inauguration in 1989. Fifteen of these missions used the SRMU rather than its predecessor, the SRM [12]. The internal geometry of the SRMU is shown in Fig. 1 as a function of burn time.

A. Motor Head End Pressure

On every Titan IV flight, both SRMUs have a pressure transducer at the head end of the combustion chamber. These measurements are acquired at 400 samples per second and include both the quasi-steady and oscillatory components of the pressure.

A waterfall plot of power spectral density for the SRMU 1 pressure oscillation history is shown in Fig. 2. The 14–21 Hz frequency range encompasses the organized pressure oscillations centered around the first axial acoustic mode of the motor chamber [13].

The SRMU ground tests included an analog measurement of purely oscillatory pressure (i.e., without a quasi-steady component) as well as a digital measurement similar to that acquired in Titan IV flight. The former was used for the data analyses presented in [13]. Comparisons of spectra for the two measurements reveal that harmonics of the 14–21 Hz content are evident in the analog measurement but that, particularly towards the end of the motor burn, the spectral amplitudes of these harmonics fall well below the

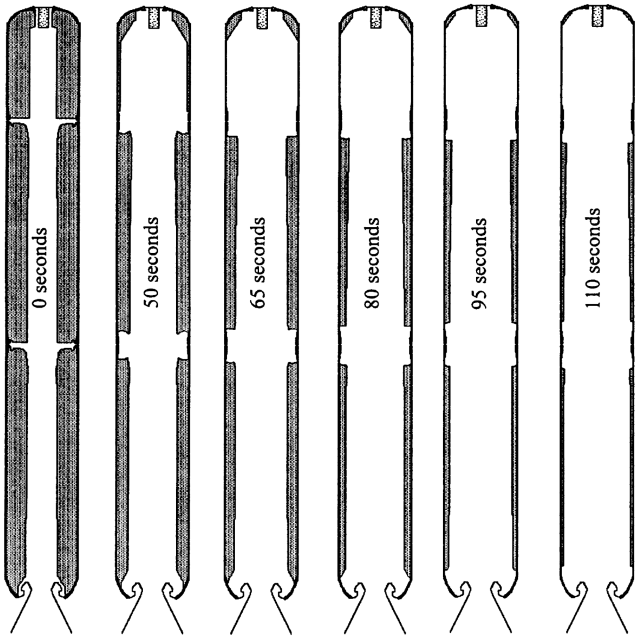

Fig. 1 SRMU internal geometry during burn.

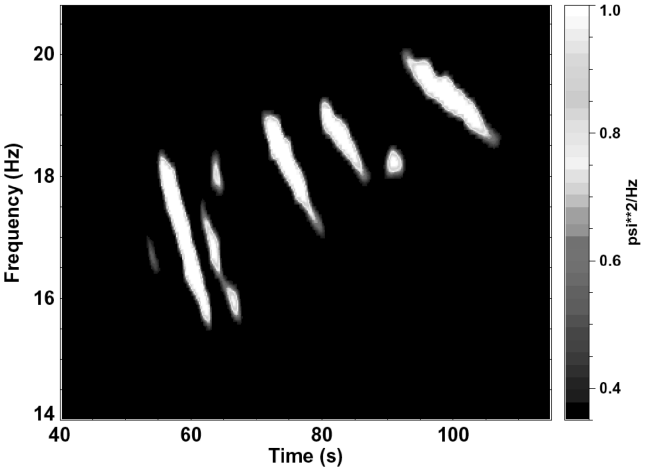

Fig. 2 Waterfall plot of power spectral density for SRMU head end pressure.

0.02 psi^2/Hz noise floor of the digital measurement. Fluid–structure interaction in Titan IV SRMU flight data, therefore, can only be assessed over the frequency range 14–21 Hz.

B. Motor Structural Acceleration

Structural accelerations are measured during Titan IV flights on a different data acquisition system than that used for the motor pressure measurements. Timing between the two systems, however, can be correlated for some flights because of a colocated measurement on the two systems.

Of the 15 Titan IV flights with SRMUs, seven had axial and tangential accelerometers mounted at the motor head and aft ends. Like the SRMU head end pressure transducers, the axial accelerometers measure both the quasi-steady and oscillatory components. The amplitude resolution of the digital signal equals 0.042 g, and 400 samples are recorded every second.

A time history of SRMU 1 head end axial acceleration is shown in Fig. 3. These acceleration data and the pressure data shown in Fig. 2 were acquired during the same Titan IV flight.

A response blossom is evident in Fig. 3 around 100 s. This time period does not correspond to a flight event that was expected based on SRMU ground test experience. The response blossom around

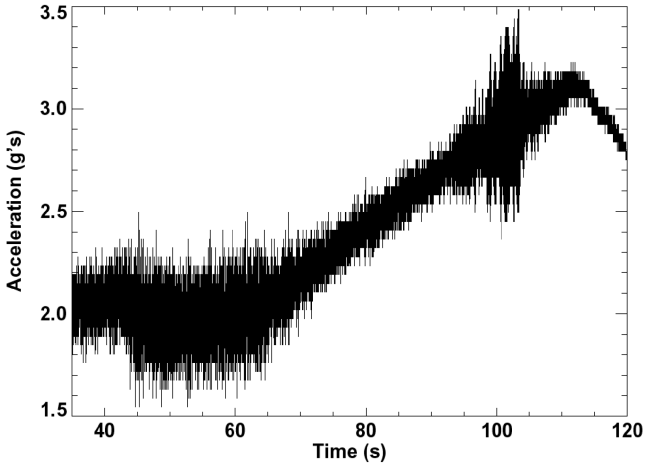

Fig. 3 Flight measurement of SRMU head end axial acceleration.

100 s also appears in the other Titan IV missions with SRMU accelerometers and is, hence, systematic and repeatable. The response amplitude for SRMU 1 in Fig. 3 is the largest among the 14 motors on the seven missions with SRMU accelerometers.

A waterfall plot of power spectral density for the SRMU 1 head end accelerometer measurement is provided in Fig. 4. Comparison of Figs. 2 and 4b confirms that the accelerations in the 14–21 Hz range are related to the motor oscillatory pressure. The largest pressure oscillations in this frequency range occur around 58 s, but do not induce significant axial structural responses. However, the motors *do* respond to lower-amplitude pressure oscillations about 40 s later.

Figure 4a also shows that around 100 s the motor structural response appears to include two harmonics of the 14–21 Hz content. The signal-to-noise ratio of the head end pressure measurement precludes detection of this content, but the character of the frequency tracks in Fig. 4a strongly suggests that the accelerations centered around 40 and 60 Hz are attributable to harmonics of the oscillatory pressure frequencies shown in Fig. 2.

Data analyses indicate that the SRMU 1 and SRMU 2 head end axial accelerations are uncorrelated, and that the same is true for the SRMU 1 and SRMU 2 pressure oscillations. It can, therefore, be concluded that the flight motors do not interact, and that the SRMU 1 and SRMU 2 flight measurements are statistically independent. This conclusion doubles the number of samples in the Titan IV flight data family that can be plotted to assess pressure amplitude probability.

C. Comparisons with Ground Test Data

During fluid–structure interaction, structural motion has a corresponding effect on oscillatory pressure. That is, feedback between the motor pressure and structural responses may decrease the effective damping of the acoustic mode [Eq. (2)]. A decrease in effective damping due to interactions with the structure can be expected to yield pressure oscillation amplitudes that are higher than those in the absence of such interactions.

Sample calculations in [7] show that structural–acoustic interaction tends to increase pressure oscillations, particularly when the acoustic and structural frequencies are similar. Hessler and Glick [6] also note that the pressure oscillations measured in ground tests and launch vehicle flight can be different because the structural modes in the ground test and flight configurations are generally different. In this section, ground test pressure measurements are analyzed to assess this possibility for the SRMU.

Figure 5 compares peak-to-peak amplitudes and rms values for flight and ground test head end pressure measurements. A 14–21 Hz band pass filter has been applied, and the data are grouped into the periods $t < 70$ s and $t > 70$ s. It is shown in the next section that during flights of the Titan IV the effects of fluid–structure interaction appear to be minimal during the former period and conspicuous during the latter.

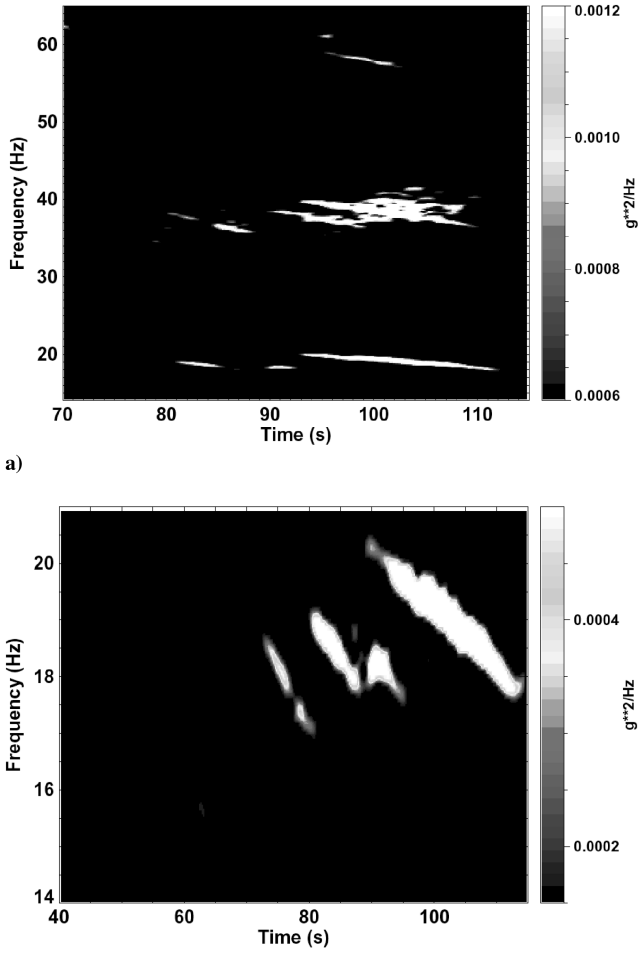

Fig. 4 Waterfall plot of power spectral density for head end axial acceleration.

Figure 5 shows that the ground test and flight data are in reasonable agreement during the period $t < 70$ s, but that fluid–structure interaction appears to amplify the pressure oscillations during the period $t > 70$ s. The average peak-to-peak amplitude and rms value are 20 and 26% higher, respectively, for the flight data during the period $t > 70$ s. It should be noted, however, that fluid–structure interaction did not cause the overall envelope of SRMU pressure oscillation amplitudes to be larger than those measured in ground tests; the largest amplitudes in the 14–21 Hz range occurred before the interaction effects became pronounced. Consequently, the structural dynamic analyses conducted with forcing functions derived from ground test pressure oscillations still conservatively predicted the Titan IV flight loads due to this phenomenon.

IV. Numerical Assessments of Interactions

A procedure for establishing the relationship between motor pressure and structural acceleration is described in this section. The procedure is then applied to the Titan IV SRMU data to show that fluid–structure interaction occurred during the period $t > 70$ s.

A. Time-Varying Amplitude and Phase

For an acceleration signal $a(t)$, we shall consider the analytic signal $z_a(t) = a(t) + i\hat{a}(t)$, where $\hat{a}(t)$ is the quadratic component defined by the Hilbert transform of $a(t)$ [14]. Expressing $z_a(t)$ in polar form, we obtain

$$z_a(t) = A_a(t)e^{i\theta_a(t)} \tag{3}$$

where

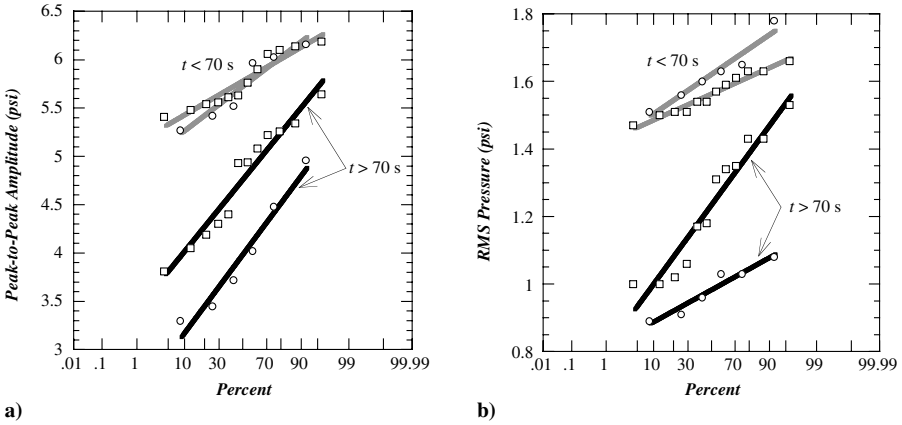

Fig. 5 Gaussian probability plots for ground test (circles) and flight (squares) pressure oscillations.

$$A_a(t) = \sqrt{a^2(t) + \hat{a}^2(t)} \quad \text{and} \quad \theta_a(t) = \arctan\left[\frac{\hat{a}(t)}{a(t)}\right] \tag{4}$$

are the time-varying amplitude and phase, respectively, of $z_a(t)$.

If $a(t)$ is a zero-mean narrowband signal with a single time-varying frequency component, the instantaneous frequency of $a(t)$ is defined by [15]

$$\omega_a(t) = \frac{\mathrm{d}}{\mathrm{d}t}\theta_a(t) \tag{5}$$

Similarly, the analytic extension of a narrowband motor pressure can be represented by

$$z_p(t) = A_p(t)e^{i\theta_p(t)} \tag{6}$$

and

$$\omega_p(t) = \frac{\mathrm{d}}{\mathrm{d}t}\theta_p(t) \tag{7}$$

During fluid–structure interaction, the axial structural acceleration and motor pressure can be characterized by quasi-sinusoidal signals with slowly varying amplitudes and essentially constant phase differences. During periods of strong interaction,

$$\omega_a(t) \sim \omega_p(t) \quad \text{and} \quad \theta_p(t) - \theta_a(t) \approx \frac{\pi}{2} \tag{8}$$

The methodology described in this section for the determination of instantaneous frequency, amplitude, and phase has been applied during assessments of fluid–structure interaction in liquid rocket engines to establish the time periods of pogo stability and instability [16].

B. Application to Titan IV SRMU Data

This section concentrates on application of the Hilbert transform over the frequency range 14–21 Hz, which corresponds to pressure oscillations in the vicinity of the first axial acoustic mode.

A Chebyshev Type I filter with six poles was applied to the pressure and acceleration measurements [17]. The filter was applied both forward and backward to remove phase distortion. The sign of the acceleration measurement was also reversed to be consistent with positive pressure and thrust oscillations. The results from application of the Hilbert transform are shown in Fig. 6. The plotted frequency, magnitude, and phase values at a given time point equal the average values over a 3-s window centered about that time point.

Frequencies of the motor head end pressure and axial acceleration are shown in Fig. 6a. The difference between these frequency histories is shown in Fig. 6b. It is evident that the two frequencies coincide only intermittently around the time of the maximum pressure oscillations, but tend to overlay during the latter part of the motor burn. The frequency histories are most strongly correlated during the period 73–107 s. Spikes in the frequency difference history occur at the changes in the vortex shedding stage number [13], and are caused by numerical uncertainty at these discontinuities.

Figure 6d shows that the acceleration oscillations always lead the pressure oscillations during the 73–107 s period. The phase difference falls in the range 23–69 deg, with an average value of 47 deg.

C. Phase Analysis

The significance of the near-constant phase values in Fig. 6d is more readily understood when phase is related to structural velocity and motor thrust, as follows. The equation of motion for a single stationary structural mode is analogous to that for a single stationary acoustic mode [Eq. (1)], namely,

$$\ddot{q} + 2\zeta_o\omega_o\dot{q} + \omega_o^2 q = f'(t) + f'(q, \dot{q}, \ddot{q}) \tag{9}$$

Let the force and response amplitudes be quasi steady. Then,

$$q(t) \sim \bar{q}\sin\omega t, \qquad \dot{q}(t) \sim \bar{q}\omega\cos\omega t \sim \dot{\bar{q}}\cos\omega t \tag{10a}$$

$$f'(q, \dot{q}, \ddot{q}) \sim \bar{f}\sin(\omega t + \theta) \tag{10b}$$

where the instantaneous frequency ω is defined by the tracks in Fig. 6a. Equation (9) can now be expressed as

$$\ddot{q} + 2\zeta_e\omega_e\dot{q} + \omega_e^2 q = f'(t) \tag{11}$$

where

$$\omega_e \sim \omega_o\sqrt{1 + (\bar{f}/\bar{q})\sin\phi/\omega_o^2} \tag{12a}$$

$$\zeta_e \sim \frac{\zeta_o - (\bar{f}/\dot{\bar{q}})\cos\phi/2\omega_o}{\sqrt{1 + (\bar{f}/\bar{q})\sin\phi/\omega_o^2}} \tag{12b}$$

and $\phi = \theta - 90$ deg is the phase difference between the pressure and structural velocity.

Equation (11) shows that, when feedback occurs, the motor structure behaves like an oscillator, with modified frequency and damping values, subjected to forces that are independent of pressure.

Figures 6c and 6d indicate that the amplitude ratios in Eq. (12) are slowly varying and that the phase difference is nearly constant over the period 73–107 s. The effective frequency and damping values, therefore, appear to be slowly varying during SRMU fluid–structure interaction.

Equation (12b) indicates that the phasing between structural velocity and pressure can have a significant impact on effective damping; the strongest reduction in damping occurs when these histories are perfectly in phase. Negative values of effective damping are possible, and yield a modal response q that grows at an

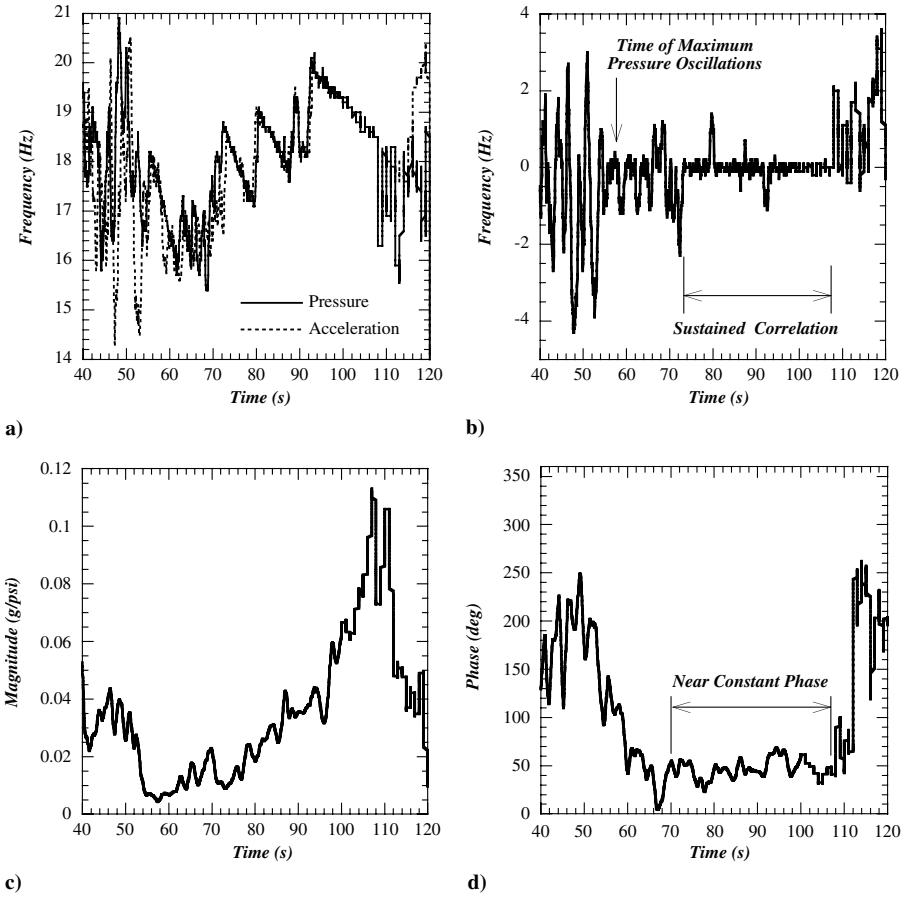

Fig. 6 Application of Hilbert transform to 14–21 Hz pressure and acceleration flight data.

exponential rate. Effective damping identically equal to zero corresponds to forced oscillations that vary about a limit cycle state.

According to Fig. 6d, the average phase difference ϕ between the SRMU structural velocity and force equals 53 deg (90 − 47 deg), where force leads velocity; the instantaneous phase difference, however, is sometimes as low as 21 deg. To visualize the phasing between structural velocity and pressure, the SRMU flight structural acceleration was integrated; this derived velocity is compared with the SRMU flight pressure oscillations in Fig. 7, in which the histories have been normalized to accommodate a single amplitude scale.

For the 2 s window of data shown in Fig. 7, the phase difference between structural velocity and pressure equals approximately 36 deg (90 − 54 deg). Therefore, the pressure history leads the velocity history in this window by (on average) one-tenth of one cycle, or approximately 5 ms.

Because positive axial pressure produces positive axial thrust, it is evident that a significant component of the SRMU thrust is in phase with structural velocity during the late burn times. Equation (12b) indicates that, provided a single stationary structural mode is involved, the SRMU phase relationship significantly reduces effective damping during the fluid–structure interaction.

V. Structural Modeling

The response blossom evident in Fig. 2 around 100 s does not correspond to an expected flight event. Accelerometers mounted on the Titan IV payload fairing, spacecraft, and first and second stages, moreover, do not indicate significant responses at this flight time. It may be concluded that the response blossom in Fig. 2 is caused by the behavior of the SRMU alone.

Finite element analyses were conducted to establish the SRMU structural characteristics. The modeling effort accounted for changes in the propellant geometry with burn time, pressure stiffening effects, and a wide range of propellant modulus.

The SRMU finite element model indicates that, in the period 80–110 s, axial modes exist with out-of-phase motion of the motor

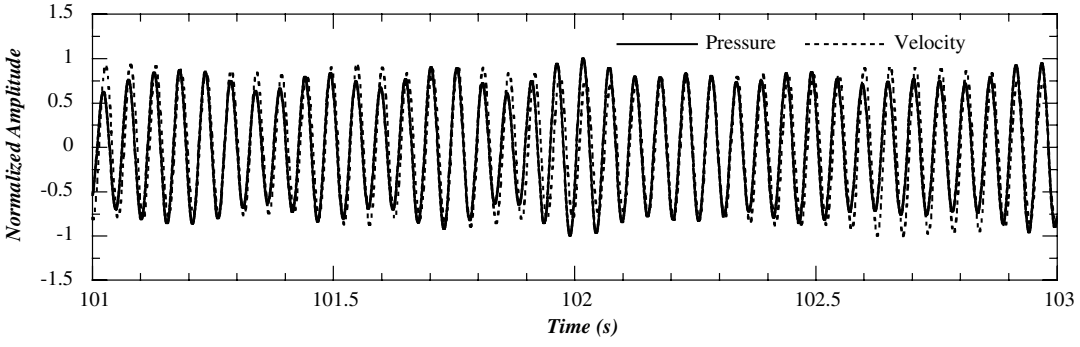

Fig. 7 Comparison of structural velocity and pressure oscillations during flight.

forward and aft ends. These modes have natural frequencies in the range 32–39 Hz. This finding is consistent with the phasing of flight accelerations and suggests that the motor structural responses between 35 and 40 Hz (see Fig. 4a) are caused by excitation of elastic axial modes.

Flight accelerations, furthermore, suggest that the 14–21 Hz component of the structural response (see Fig. 4b) corresponds to rigid body motion of the motor case. It was postulated that, in this frequency range, a structural mode of the propellant (with motion relative to the motor case) exists which couples to the motor internal flow and, hence, induces the fluid–structure interaction evident between 73 and 107 s. Figure 1, however, illustrates that little propellant remains during this time period. Indeed, the finite element model did not yield a structural mode in the frequency range 14–21 Hz, which involves motion of the propellant relative to the motor case. The nature of the interaction between the SRMU internal flow and structure remains unclear.

VI. Conclusions

Traditional solid rocket stability codes do not account for feedback between motor internal flow and structural responses. The fluid–structure interaction evident in Titan IV flight measurements, and the amplification of pressure oscillations relative to ground tests, suggest that coupling between the motor structure and acoustic system should not be ignored in stability predictions. Similarly, structural dynamic analyses that compute flight loads using forcing functions based solely on ground test pressure measurements should be approached with caution.

Because the interest in solid rocket motor pressure oscillations is ostensibly driven by concerns about structural integrity, the goals of motor stability analyses should include the prediction of pressure oscillation amplitudes, not simply the times of occurrence of the pressure oscillations or their initial exponential growth rate. The complete elimination of pressure oscillations in large solid rocket motors is difficult to achieve, and the prediction of flight loads induced by motor pressure oscillations require statistical assessments of pressure oscillation amplitudes.

References

[1] Majdalani, J., Flandro, G. A., and Fischbach, S. R., "Some Rotational Corrections to the Acoustic Energy Equation in Injection-Driven Enclosures," *Physics of Fluids*, Vol. 17, No. 7, 2005, pp. 7410201–7410220.

[2] Nickerson, G. R., Culick, F. E. C., and Dang, A. L., "Solid Propellant Rocket Motor Performance Computer Program (SPP), Version 6.0," Air Force Astronautics Lab, TR-87-078, Edwards AFB, CA, Dec. 1987.

[3] Flandro, G. A., Majdalani, J., and French, J. C., "Incorporation of Nonlinear Capabilities in the Standard Stability Prediction Program," AIAA Paper 2004-4182, July 2004.

[4] Flandro, G. A., Fischbach, S. R., Majdalani, J., and French, J. C., "Nonlinear Rocket Motor Stability Prediction: Limit Amplitude, Triggering, and Mean Pressure Shift," AIAA Paper 2004-4054, July 2004.

[5] Dotson, K. W., Womack, J. M., and Grosserode, P. J., "Structural Dynamic Analysis of Solid Rocket Motor Resonant Burning," *Journal of Propulsion and Power*, Vol. 17, No. 2, 2001, pp. 347–354.

[6] Hessler, R. O., and Glick, R. L., "Comment on Dotson et al. 'Structural Dynamic Analysis of Solid Rocket Motor Resonant Burning'," *Journal of Propulsion and Power*, Vol. 21, No. 1, 2005, pp. 190–191.

[7] Deur, J. M., and Hessler, R. O., "Forced Oscillation Theory," AIAA Paper 84-1356, June 1984.

[8] Dotson, K. W., "Reply to Technical Comment by R. O. Hessler and R. L. Glick," *Journal of Propulsion and Power*, Vol. 21, No. 1, 2005, pp. 191–192.

[9] Hessler, R. O., "Passive Linear Stability Measurements," *Joint Army-Navy-NASA-Air Force (JANNAF) Propulsion Meeting*, CPIA Publ. 662, Vol. 2, Chemical Propulsion Information Agency, Columbia, MD, 1997, pp. 163–176.

[10] Majdalani, J., Vyas, A. B., and Flandro, G. A., "Higher Mean-Flow Approximation for Solid Rocket Motors with Radially Regressing Walls," *AIAA Journal*, Vol. 40, No. 9, 2002, pp. 1780–1788.

[11] Majdalani, J., and Flandro, G. A., "The Oscillatory Pipe Flow with Arbitrary Wall Injection," *Proceedings of the Royal Society of London, Series A*, Vol. 458, No. 2022, 2002, pp. 1621–1651.

[12] Isakowitz, S. J., Hopkins, J. P., Jr., and Hopkins, J. B., *International Reference Guide to Space Launch Systems*, 3rd ed., AIAA, Washington, DC, 1999, pp. 447–470.

[13] Dotson, K. W., Koshigoe, S., and Pace, K. K., "Vortex Shedding in a Large Solid Rocket Motor Without Inhibitors at the Segment Interfaces," *Journal of Propulsion and Power*, Vol. 13, No. 2, 1997, pp. 197–206.

[14] Papoulis, A., *Signal Analysis*, 1st ed., McGraw–Hill, New York, 1977.

[15] Huang, N. E., "A New Method for Nonlinear and Nonstationary Time Series Analysis: Empirical Mode Decomposition and Hilbert Spectral Analysis," *Wavelet Applications VII, Proceedings of SPIE*, Vol. 4056, SPIE, Bellingham, WA, 2000, pp. 197–209.

[16] Dotson, K. W., Rubin, S., and Sako, B. H., "Mission-Specific Pogo Stability Analysis with Correlated Pump Parameters," *Journal of Propulsion and Power*, Vol. 21, No. 4, 2005, pp. 619–626.

[17] Antoniou, A., *Digital Filters: Analysis, Design, and Applications*, McGraw–Hill, New York, 1993, pp. 249–273.

S. Son
Associate Editor